Effect of Nose Bluntness on Flowfield Over Slender Bodies in Hypersonic Flows

D. J. Singh*
Old Dominion University, Norfolk, Virginia 23529
A. Kumar†
NASA Langley Research Center, Hampton, Virginia 23665
and
S. N. Tiwari‡
Old Dominion University, Norfolk, Virginia 23529

A parametric study has been conducted to determine the effects of nose bluntness on the entire flowfield over slender bodies under different hypersonic freestream conditions. The slender bodies considered are blunted cones and ogives. The analysis is carried out for air under perfect- and equilibrium-gas assumptions. The analyses range from a few simplified approaches to the solution of the complete Navier-Stokes equations. The numerical procedures are based on the solution of the Navier-Stokes and parabolized Navier-Stokes equations. Specific results obtained for spherically blunted cones and ogives demonstrate that there are significant differences in flowfield and surface quantities between sharp and blunted bodies. Depending upon the flow conditions and geometry, the differences are found to persist as far as 260 nose radii downstream.

Nomenclature

C_f = coefficient of skin friction
C_h = coefficient of heat transfer
$\dot{m}$ = mass flow rate
M = Mach number
P = pressure
Pr = Prandtl number
Q_w = wall heat transfer, nondimensionalized by $\rho_\infty U_\infty^3$
Re = Reynolds number
R_n = nose radius
T = temperature
u = axial velocity
x = streamwise coordinate in physical domain measured from virtual tip of sharp nose
y = normal coordinate in physical domain
δ_{sh} = shock standoff distance
ρ = density
θ_c = cone angle

Subscripts
e = local conditions at the boundary-layer edge
∞ = freestream conditions
w = conditions at the body surface

Introduction

THERE is a renewed interest in the hypersonic flow regime after a period of over a decade primarily because of the proposed National Aerospace Plane. This hypersonic aircraft is to be powered by an air-breathing engine, which has to be very closely integrated with the airframe to avoid severe drag penalties. In the analysis of the engine flowfield, the forebody flow provides the initial conditions. It is, therefore, necessary to accurately predict the forebody flowfield by incorporating realistic conditions and geometrical modeling. One of the geometrical features that can have significant effect on the entire flowfield is the nose bluntness. In hypersonic flow over slender bodies, the influence of nose bluntness can be significant for hundreds of nose dimensions downstream. Thus, it is important to develop efficient and reliable methods for predicting the effects of the blunt nose on the entire flowfield.

In most studies involving flow past slender bodies, it is assumed that the leading edge is infinitely sharp. In practice, it is impossible to manufacture a body with zero leading-edge thickness since all bodies must have some finite bluntness in order to sustain the heat generated at hypersonic speeds. Early studies on the effects of nose blunting are summarized in classical books on hypersonic flows.[1-5] An extensive literature survey on the bluntness and viscous interaction effects on slender bodies at hypersonic speeds is provided by Dewey.[6] Some studies that have been carried out for flat plates[7-11] and slender bodies[12-19] are limited to a very small nose bluntness and rarefied flows. In recent years, certain numerical and experimental efforts have been directed to investigate the effects of nose bluntness on slender bodies.[20-29]

The objective of the present study is to conduct a parametric study to investigate the effects of nose bluntness on the entire flowfield past slender bodies under different physical and

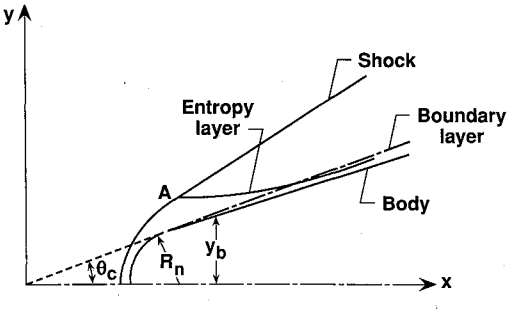

Fig. 1 Physical model for hypersonic flow past a blunted cone.

Presented as Paper 89-0270 at the AIAA 27th Aerospace Science Meeting, Reno, NV, Jan. 9-12, 1989; received March 20, 1989; revision received Feb. 22, 1990.

*Graduate Research Assistant, Department of Mechanical Engineering and Mechanics. AIAA Student Member. Present Affiliation: Analytical Systems and Material Inc., Hampton, VA.

†Head, Theoretical Flow Physics Branch, Fluid Mechanics Division. Associate Fellow AIAA.

‡Eminent Professor, Department of Mechanical Engineering and Mechanics. Associate Fellow AIAA.

Table 1 Flow conditions

Quantity	$M_\infty = 10$	$M_\infty = 20$
P_∞, N/m^2	404.7	171.0
T_∞, K	243.4	261.3
T_{wall}, K	1000	1000
Pr	0.72	0.72

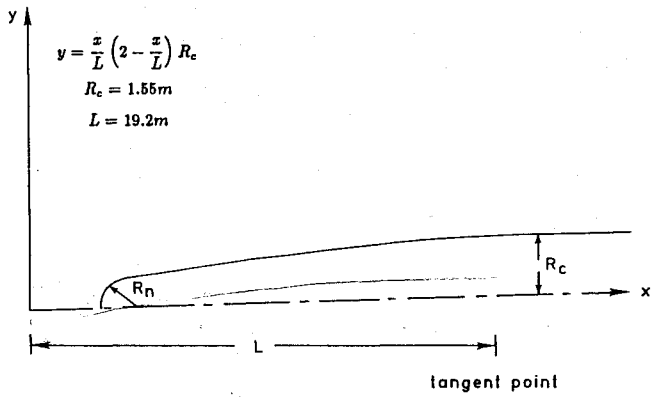

Fig. 2 Physical model for hypersonic flow past an ogive.

freestream conditions. The slender bodies considered are blunted cones and other bodies of revolution. Approximate engineering methods and accurate computational procedures are used to obtain specific results.

Physical Model and Analytical Procedure

The physical model for hypersonic flow past a blunt-nosed slender body is shown in Fig. 1. The relative positions of boundary, entropy, and shock layers are indicated in the figure. The first physical problem considered is the flow past a blunt-nosed slender cone. Numerical results have been obtained by employing the combination of a Navier-Stokes code and a parabolized Navier-Stokes code. These are discussed here briefly and some specific results are presented in subsequent sections.

In the present study, 5-, 10-, and 20-deg half-angle cones are selected first with spherical nose tip as shown in Fig. 1. Three nose tips with radius of 0.0025 m, 0.025 m, and 0.05 m are considered, with the smallest nose-radius tip approximating the sharp tip. Blunting was accomplished by keeping the cone angle fixed and increasing the nose radius. The bluntness effects are determined by comparing the solutions obtained from the blunted tips with that obtained from the sharp tip. As shown in Fig. 1, the origin of the coordinate system is at the virtual tip of the sharp cone with x axis along the symmetry line and y axis normal to it. The second geometry considered is a generic forebody (Fig. 2) with three nose tips of the same radii as the cone. Here again the smallest nose radius approximates the sharp-tip body.

For the spherical nose region of the body, the flow is analyzed by the code SOFIA,[30] which is a finite-volume, Navier-Stokes code based on a time-dependent adaptive grid algorithm. Use of full Navier-Stokes equations is necessary around the nose due to the subsonic flow in this region, but slightly downstream of the nose region on the body, the flow becomes predominantly supersonic and a space marching code can be used to analyze the flow. In the present investigation, a parabolized Navier-Stokes code developed by Vigneron et al.[31] and subsequently modified by Gnoffo[32] is used for analyzing the downstream flow over the bodies. The details of the governing equations and method of solution are given Refs. 30 and 31. It should be noted that throughout the present study, flowfield is assumed to be laminar. The freestream conditions used are given in Table 1. These conditions correspond to the two trajectories for the proposed National Aerospace Plane.

Validation

The program was validated by comparing the present results with those calculated using the laminar theory with the reference temperature concept.[33] For the same Reynolds number, the skin friction on a cone and a flat plate is related by

$$C_{f,\text{cone}} = \sqrt{3} C_{f,\text{plate}} \tag{1}$$

Using the Reynolds analogy, the heat transfer coefficient is expressed as[33]

$$C_{h,\text{cone}} = \frac{C_{f,\text{cone}}}{2Pr^{2/3}} \tag{2}$$

The value of $C_{f,\text{plate}}$ can be calculated from

$$C_{f,\text{plate}} = \frac{0.664\sqrt{C^*}}{\sqrt{Re_{xe}}} \tag{3}$$

where Re_{xe} is the Reynolds number based upon the distance along the cone surface and C^* is the reference viscosity given by the Sutherland's law as

$$C^* = \left(\frac{T^*}{T_e}\right)^{0.5} \frac{T_e + K}{T^* + K} \tag{4}$$

where $K = 200°$R and

$$T^*/T_e = 0.5 + 0.039M_e^2 + 0.5(T_w/T_e)$$

By using Eqs. (1-3), we can calculate theoretical values of $C_{f,\text{cone}}$ and $C_{h,\text{cone}}$. The subscript e refers to the edge conditions. The edge conditions were obtained from Taylor-Maccoll theory.[34] These results are compared with the numerically

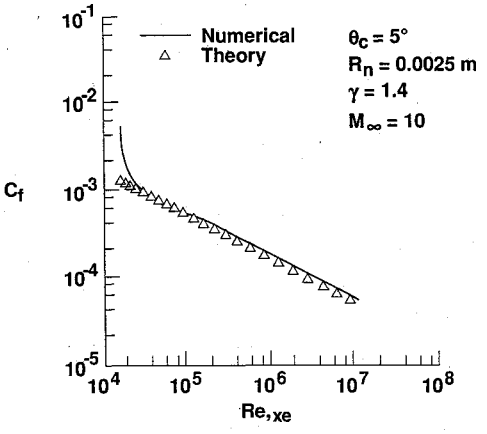

Fig. 3 Comparison of skin-friction coefficient with laminar theory.

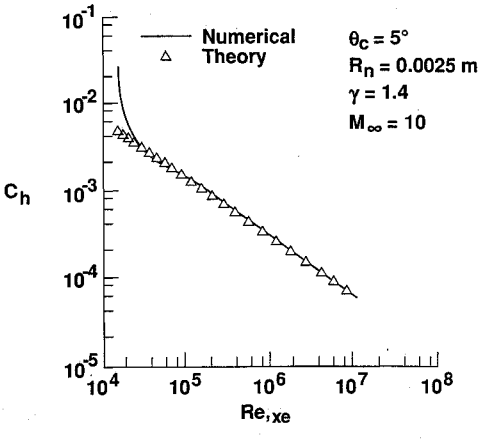

Fig. 4 Comparison of heat transfer coefficient with laminar theory.

Table 2 Entropy-swallowing distance (x/R_n) for 5-deg cone at $M_\infty = 10$

R_n	Reynolds number	Present	Rotta
0.0025	2891	139	224
	14,454	206	375
0.025	22,908	243	470
	57,816	286	590
0.05	57,816	288	590

calculated values for sharp cone at $M_\infty = 10$ in Figs. 3 and 4. The results show a very good comparison. The surface pressure and shock standoff distance, when compared with inviscid values, also show excellent agreement.

Entropy Layer

Nose bluntness at hypersonic speed causes the shock wave to be detached and curved in the nose region. The changing shock curvature generates a layer of flow with entropy gradient, known as entropy layer, which "influences" the development of the boundary layer in two different ways. First, it causes a continuous change of the flow properties at the outer edge of the boundary layer in the streamwise direction; and second, it produces a velocity and pressure gradient at the outer edge. These external gradients invalidate the classical boundary-layer approach. However, Ferri[35] pointed out that these gradients are important when the vorticity of the inviscid flow is of the same order as that of the boundary layer. These conditions may exist when the Reynolds number is low and the Mach number is high. The thickness of the entropy layer is a function of the leading-edge bluntness; even a small leading-edge thickness generates an entropy layer that influences the local flow conditions for a large distance downstream. This entropy layer is eventually swallowed by the boundary layer in the case of flow past cones. This distance is called the entropy-swallowing distance. For conical flows, the entropy-swallowing distance is defined[24] as "the location at the cone frustrum where fluid, which has gone through the strong portion of the bow shock, has been swallowed by the boundary layer." This is by no means a precise definition as it depends upon the shock shape, boundary-layer assumptions, and definition of the entropy-layer thickness.

For hypersonic flows over a blunted slender cone, the curvature of the shock produces the entropy layer as shown in Fig. 1. Once the shock attains conical shape, it is no longer curved and hence the entropy gradient is zero. The thickness of the entropy layer decreases as it moves downstream on the body and eventually it is swallowed by the boundary layer. The entropy effects in the boundary layer vanish asymptotically further downstream.

In the present study, the entropy-swallowing distance is calculated by consideration of the mass flow rate. The entropy-layer thickness is calculated in the downstream region, and the point where the entropy-layer thickness becomes equal to the boundary-layer thickness is termed as the entropy-swallowing point. To estimate the thickness of the entropy layer, its edge is defined as the streamline that passes through the point A (Fig. 1) at which the shock attains the conical angle. Most of the entropy changes occur before this point. The rate of mass flow in the entropy layer is given by

$$\dot{m} = 2\pi \int_{y_b}^{y_e} \rho u y \, dy \tag{5}$$

At point A, the mass flow rate is expressed as

$$\dot{m}_A = \pi y_A^2 \rho_\infty U_\infty \tag{6}$$

Since the mass flow rate between the body and the streamline passing through point A is known [Eq. (6)], the locus of point A can be calculated using Eqs. (5) and (6), with $y_e(x)$ as the only unknown. Other methods for calculating the entropy-swallowing distances are discussed in Ref. 38.

A comparison of the entropy-swallowing distance with the results of Rotta[36] for Mach 10 freestream conditions (Table 1) is given in Table 2 for various nose bluntness and Reynolds numbers. The table shows a large difference between the present results and the empirical results of Rotta. This difference increases with the increasing bluntness. As will be shown later, the present approach for calculating the entropy-swallowing distance agrees qualitatively with the merging distance for skin friction, surface pressure, wall heat transfer, and shock shape. The theoretical calculations of Rotta assume that the pressure on the conical portion of the body is constant, and, therefore, the overexpansion and recompression on the shoulder are neglected. Also a correlation for the shock shape is used. The errors introduced by these approximations increase with the increase in nose bluntness. Thus, Rotta's results are valid only for very small values nose of bluntness.

Equilibrium Chemistry

To include the real-gas effects that might be present at hypersonic speeds, calculations are also made with equilibrium air chemistry. The equilibrium chemistry package developed in Ref. 37 is used in the analysis. It is based upon the free-energy minimization technique and has been implemented by Gnoffo[30,32] into the Navier-Stokes and parabolized Navier-Stokes codes.

Results and Discussion

Extensive results have been obtained for various freestream conditions given in Table 1 and for three different values of

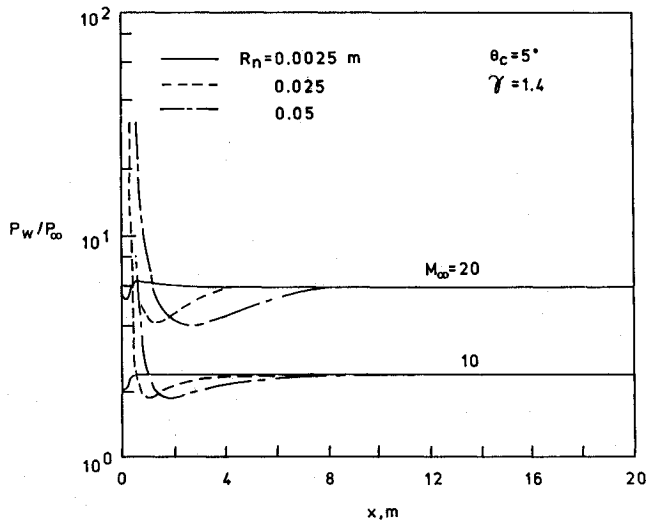

Fig. 5 Variation of wall pressure with the axial distance for $\theta_c = 5$ deg at various Mach numbers.

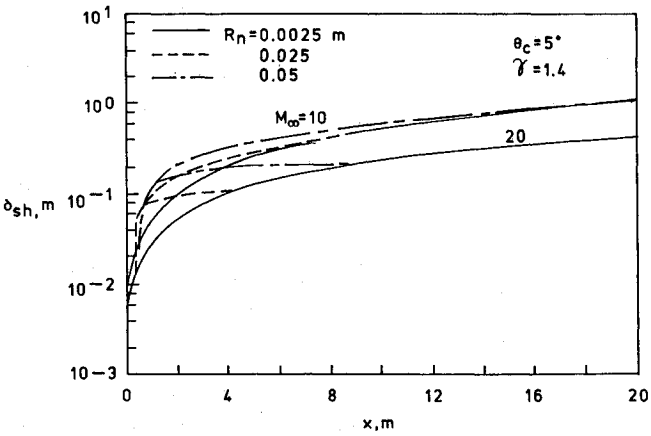

Fig. 6 Variation of shock-standoff distance with the axial distance for $\theta_c = 5$ deg at various Mach numbers.

nose bluntness. Some typical results are presented here. As mentioned earlier, the blunted cone with smallest nose radius is considered as a sharp cone and the effects of leading-edge bluntness is compared with respect to this cone. When the surface quantities fall within 5% of the sharp-cone values, the effect of bluntness is assumed to have vanished. The same criterion is also used for the case of ogive.

Figures 5–7 show the variation of surface quantities with the axial distance for a 5-deg cone with various degrees of bluntness and for freestream Mach numbers of 10 and 20. The x distance is measured from the virtual tip of the sharp cone. The results are plotted downstream of the sphere-cone juncture point. The surface-pressure distributions are presented in Fig. 5. The pressure has been nondimensionalized with respect to the respective freestream pressure. In the stagnation region, the pressure is very high but as the flow moves downstream, the shock strength decreases thereby decreasing the pressure. The flow overexpands near the shoulder; the extent of overexpansion is a function of the bluntness and freestream conditions. The overexpanded flow then recompresses back to the sharp-cone value. The distance it takes to reach the sharp-cone value is also a function of the freestream conditions and nose bluntness. It should be noted that the pressure on the cone is influenced by the nose over a large portion of the afterbody and is lower than the conical pressure. For all values of leading-edge bluntness considered, the surface pressures have reached the same value at about 160 nose radii downstream.

Figure 6 shows the variation of the shock-standoff distance as a function of the axial distance. The shock-standoff distances are measured from the body surface. Here the behavior of the shock shape is seen to be qualitatively similar to those observed by previous investigators.[18] The shock-standoff distance is affected considerably by the leading-edge bluntness. For the sharp cone, it is a straight line, whereas for blunted cones it is curved with an inflection point about 50 nose radii downstream. For a sufficiently large value of x, the shock shape becomes independent of nose bluntness.

The variation of the skin-friction coefficient with the axial distance is shown in Fig. 7. It is seen that the skin friction decreases over the body with increasing nose bluntness at a given Mach number. This is because the entropy layer increases the thickness of the boundary layer, thereby reducing the gradients of velocity profile near the body. The skin friction is found to be most sensitive to the nose bluntness as it takes the maximum distance to reach the sharp-cone value among all of the flow properties.

At Mach 20 freestream conditions, it takes less distance to attain the conical value than at Mach 10 conditions; this is not

Table 3 Distance (x/R_n) up to which bluntness effect persists for $M_\infty = 10$

Quantity	R_n,m	$\theta_c = 5$ deg	Ogive ($\gamma = 1.4$)
P_w	0.025	120	47
	0.05	160	48
δ_{sh}	0.025	209	63
	0.05	218	71
C_f	0.025	233	127
	0.05	267	154
Q_w	0.025	120	44
	0.05	160	48

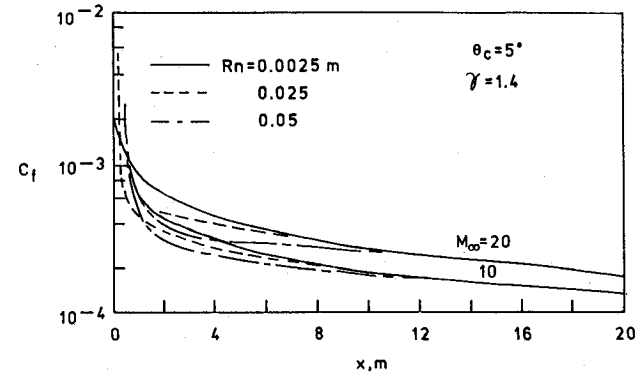

Fig. 7 Variation of skin friction with the axial distance for $\theta_c = 5$ deg at various Mach numbers.

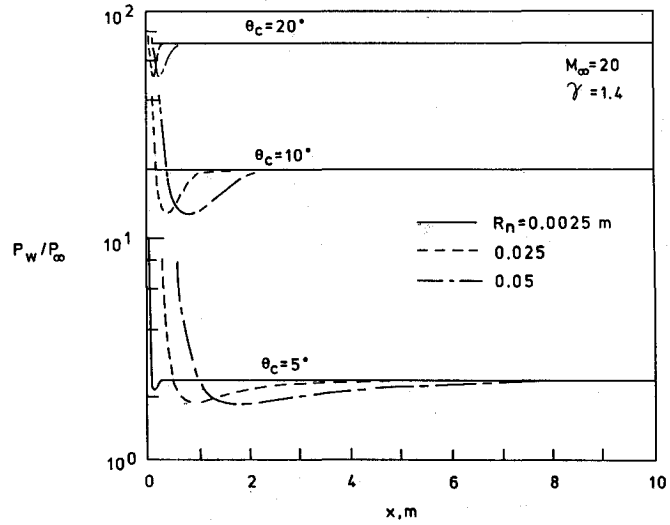

Fig. 8 Variation of wall pressure with the axial distance for $\theta_c = 5$, 10, and 20 deg at $M_\infty = 20$.

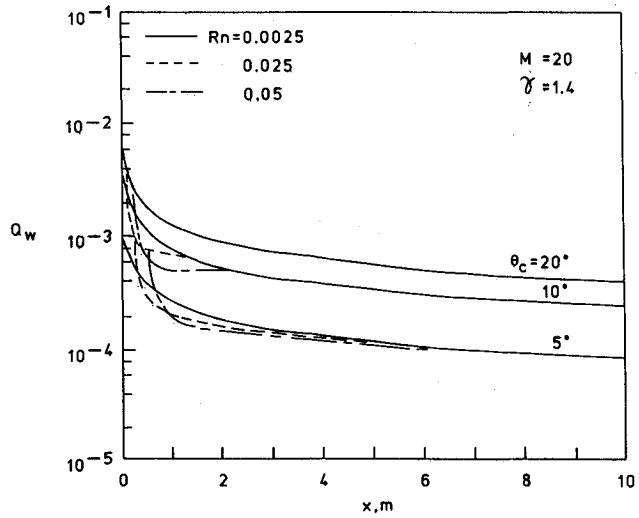

Fig. 9 Variation of wall heat transfer with the axial distance for $\theta_c = 5$, 10, and 20 deg at $M_\infty = 20$.

Table 4 Distance (x/R_n) up to which bluntness effect persists for $M_\infty = 20$

Quantity	R_n,m	$\theta_c = 5$ deg	$\theta_c = 10$ deg	$\theta_c = 20$ deg	Ogive ($\gamma = 1.4$)	Ogive (Equil.)
P_w	0.025	113	38	9	48	38
	0.05	146	40	15	52	40
δ_{sh}	0.025	172	43	10	57	44
	0.05	182	45	11	67	50
C_f	0.025	165	80	25	87	65
	0.05	198	108	35	121	119
Q_w	0.025	126	37	10	46	36
	0.05	135	40	18	50	37

to say that for the same freestream conditions the increase in Mach number will decrease the merging distance. Increasing the Mach number will increase the Reynolds number, which reduces the the boundary-layer thickness. This would increase the merging distances. The merging distances depend upon the $\rho_\infty U_\infty$ product. It should be noted that the density for Mach 20 freestream condition is 0.4 times the density at Mach 10, so the $\rho_\infty U_\infty$ product is lower at Mach 20 than at Mach 10 conditions.

The distances to attain conical values of surface pressure, shock-standoff distance, wall heat transfer, and skin friction are given in Tables 3 and 4. Similar results for ogive with various degree of bluntness show the same trend.[38]

The effects of cone angle have been investigated for a freestream Mach number of 20 and cone angles of 5, 10, and 20 deg. Some results for surface quantities are presented in Figs. 8 and 9. An interesting general trend is noticed from these figures. With a small increase in cone angle from 5 to 10 deg, the merging distances decrease dramatically. The merging distances decrease even more when the cone angle is increased from 10 to 20 deg. The merging distance is shorter for the wider cones because the normal shock flow does not have to turn through as large an angle to attain a flow direction nearly parallel to the cone and therefore more quickly negotiates the required turn. The entropy-swallowing distance is a very strong function of y_A because, physically, most of the flow in the boundary layer near the swallowing point has entered before shock attains the conical value.

The variation in the wall pressure with axial distance for various cone angles is shown in Fig. 8. The wall pressure increases with the increasing cone angle due to increased shock strength. Also the overexpansion/recompression increases with the cone angle while the physical distance over which this takes place decreases. Thus, a blunt cone with a larger cone angle will experience a constant wall pressure over most of its surface as compared to a cone with a smaller angle.

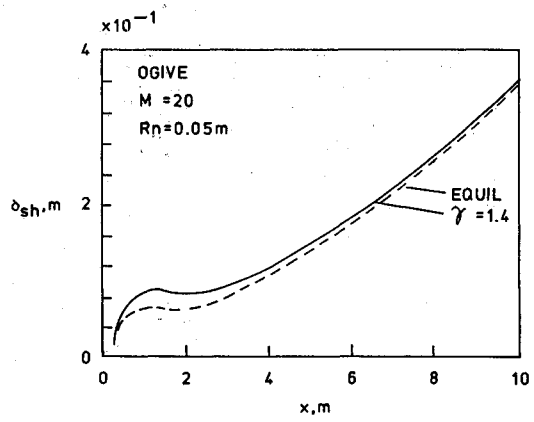

Fig. 10 Comparison of shock standoff for equlibrium and perfect gas.

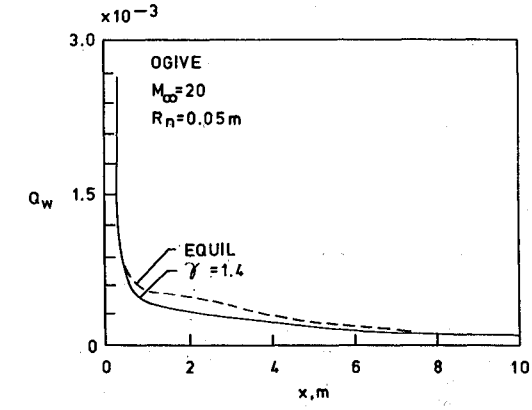

Fig. 11 Comparison of wall heat transfer equilibrium and perfect gas.

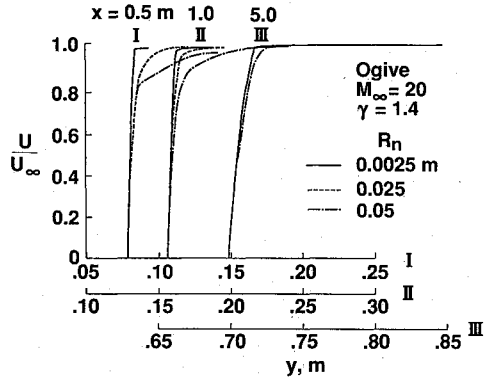

Fig. 12 Comparison of velocity profiles at $x = 0.5$, 1.0, and 5.0 m for ogive at Mach 20.

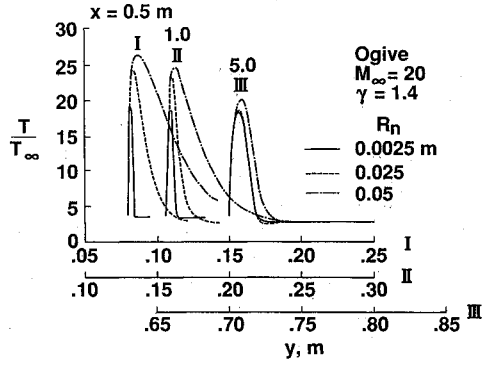

Fig. 13 Comparison of temperature profiles at $x = 0.5$, 1.0, and 5.0 m for ogive at Mach 20.

Figure 9 shows the variation of wall heat transfer for various cone angles. It shows that the heat transfer on the wall increases with increasing cone angle while merging distances decrease. Thus, larger angle cones will experience almost uniform heat transfer over most of the afterbody. These results indicate that as the cone angle increases, the extent of effects of nose bluntness decreases.

The variation of shock-standoff distance and wall heat transfer at Mach 20 for ogive of 0.05-m nose radius is shown in Figs. 10 and 11 for perfect- and equilibrium-gas flows. The equilibrium-gas results do not show any dramatic differences from the perfect-gas results although, as expected, there are some minor differences. The difference in the two solutions tends to increase with increasing Mach number and bluntness. These figures show expected effects of equilibrium-gas chemistry on the flow properties. For example, Fig. 10 shows that the shock moves closer to the body for the equilibrium gas. The merging distances for these cases are given in Table 4. Because of the shock moving closer to the body, the normal distance to attain the conical angle decreases, and thus a small decrease in merging distances is noted for equilibrium flows.

Figures 12 and 13 show the variation of the streamwise velocity and temperature as a function of y distance for Mach 20 perfect-gas flow over an ogive with various nose bluntnesses. It should be noted that since the shock-fitting procedure is used, the normal profiles are plotted within the shock layer only. The velocity and temperature have been nondimensionalized with respect to their freestream values. The variation of streamwise velocity is shown in Fig. 12 for $x = 0.5$, 1.0, and 5.0 m. These is a significant difference between the profiles near the nose; differences tend to diminish with increasing axial distance. The figure shows that the thickness of the boundary layer increases with increasing bluntness and that the shape of the profile is changed near the outer edge of the boundary layer. It is this difference that causes the wall values to be so different from the sharp-cone values. The same type of effects can be seen in Fig. 13 where

temperature profiles between shock and body are shown. Here again the differences decrease with the axial distance.

Conclusions

A parametric study has been conducted to determine the downstream effects of nose bluntness on slender bodies. The slender bodies considered are cones and ogives. Approximate methods, as well as the combination of the Navier-Stokes and parabolized Navier-Stokes equations, are used to accurately compute the flowfield. The high-temperature effects are incorporated by using the equilibrium-gas model. The effects of nose bluntness and the entropy layer generated by it are found to persist several hundred nose radii downstream depending upon the bluntness, freestream conditions, and geometry. Also the bluntness effects decrease with increasing cone angle. The results show that the wall quantities are not affected much by the inclusion of high-temperature effects through equilibrium chemistry.

References

[1]Truitt, R. W., *Hypersonic Aerodynamic*, Ronald, New York, 1959.

[2]Hayes, W. D., and Probstein, R. F., *Hypersonic Flow Theory*, Academic, New York, 1959.

[3]Chernyi, G. G., *Introduction to Hypersonic Flow*, translated from Russian by R. F. Probstein, Academic, New York, 1961.

[4]Dorrance, W. H., *Viscous Hypersonic Flow*, McGraw-Hill, New York, 1962.

[5]Cox, R. N., and Crabtree, L. F., *Elements of Hypersonic Aerodynamics*, Academic, New York, 1965.

[6]Dewey, C. F., "Bluntness and Viscous-Interaction Effects on Slender Bodies at Hypersonic Speeds," AIAA Paper 65-63, Jan. 1965.

[7]Lees, L., and Probstein, R. F., "Hypersonic Viscous Flow Over a Flat Plate," Princeton Univ., Aeronautical Engineering Dept., Princeton, NJ, Rept. 195, April 1952.

[8]Hammit, A. G., and Bogdonoff, S. M., "Hypersonic Studies of the Leading-Edge Effect on the Flow Over a Flat Plate," *Jet Propulsion*, Vol. 26, April 1956, pp. 241-246.

[9]Vas, I. E., and Bogdonoff, S. M., "An Experimental Investigation of the Flow Over Simple Two-Dimensional and Axial Symmetric Bodies at Hypersonic Speeds," *Jet Propulsion*, Vol. 26, Feb. 1958, pp. 97-104.

[10]Nagamatsu, H. T., Sheer, R. E., and Schmid, J. R., "High-Temperature Rarefied Hypersonic Flow Over a Flate Plate," *ARS Journal*, Vol. 31, July 1961, pp. 902-910.

[11]McCrosky, W. J., Bogdonoff, S. M., and McDougall, J. G., "An Experiment Model for the Sharp Flat Plate in Rarefied Hypersonic Flow," *AIAA Journal*, Vol. 4, Sept. 1966, pp. 1580-1587.

[12]Bradfield, W. S., Decouroin, D. G., and Blumer, C. G., "The Effect of Leading-Edge Bluntness on a Laminar Supersonic Boundary Layer," *Journal of the Aeronautical Science*, Vol. 21, June 1954, pp. 373-382.

[13]Lees, L., "Laminar Heat Transfer Over Blunt-Nosed Bodies at Hypersonic Flight Speeds," *Jet Propulsion*, Vol. 26, Aril 1956, pp. 259-269.

[14]Cheng, H. K., and Pallone A. J., "Inviscid Leading-Edge Effects in Hypersonic Flows," Reader's Forum, *Journal of the Aeronautical Science*, Vol. 23, July 1956, pp. 700-702.

[15]Lees, L., and Kubota, T., "Inviscid Hypersonic Flow Over Blunt-Nosed Slender Bodies," *Journal of the Aeronautical Science*, Vol. 24, March 1957, pp. 195-202.

[16]Cheng, H. K., "Similitude of Hypersonic Real-Gas Flows Over Slender Bodies with Blunted Noses," *Journal of the Aeronautical Science*, Vol. 26, Sept. 1959, pp. 575-585.

[17]Rudman, S., and Rubin, S. G., "Hypersonic Viscous Flows Over Slender Bodies with Sharp Leading Edges," *AIAA Journal*, Vol. 6, Oct. 1968, pp. 1883-1889.

[18]Stainback, R. C., "Effects of Unit Reynolds Number, Nose Bluntness, Angle of Attack, and Roughness on Transition on a 5-Deg Half-Angle Cone at Mach 8," NASA TN-D-4961, Jan. 1969.

[19]Vas, I. E., and Sierchio, J. G., "Downstream Effect of Bluntness in the Merged Flow Regime," *Rarefied Gas Dynamics*, edited by K. Karamcheti, Academic, New York, 1972, pp. 307-315.

[20]Muir, J. F., and Trujillo, A. A., "Experimental Investigation of the Effects of Nose Bluntness, Freestream Unit Reynolds Number, and Angle of Attack on Cone Boundary-Layer Transition at a Mach Number of 6," AIAA Paper 72-216, Jan. 1972.

[21]Pugh, P. G., and Ward, L. C., "A Parametric Study of the Use of Nose Blunting to Reduce the Supersonic Wave Drag of Forebodies," Aeronautical Research Council CP-1271, 1974.

[22]Ashby, G. C., Jr., and Harris, J. E., "Boundary-Layer Displacement-Thickness Effects on Zero-Lift Drag of a Series of Power-Law Bodies at Mach 6," NASA TN-D-7723, Sept. 1974.

[23]Stetson, K. F., "Mach 6 Experiment of Transition on a Cone at Angle of Attack," *Journal of Spacecraft and Rockets*, Vol. 19, No. 5, 1982, pp. 387-403.

[24]Stetson, K. F., "Nose-Tip Bluntness Effects on Cone Frustum Boundary-Layer Transition in Hypersonic Flow," AIAA Paper 83-1763, July 1983.

[25]Nowek, R. J., Albertson, C. W., and Hunt, L. R., "Aeronautical Tests of a 12.5-Deg Cone at Attack, and Nose Shapes," NASA TP-2345, Jan. 1985.

[26]Holden, M. S., "Experimental Studies of the Effects of Asymmetric Transition on the Aerothermal Characteristics of Hypersonic Blunted Slender Cones," AIAA Paper 85-325, Jan. 1985.

[27]Thompson, R. A., Zoby, E. V., Wurster, K. E., and Gnoffo, P. A., "An Aerothermodynamic Study of Slender Conical Vehicle," AIAA Paper 87-1475, June 1987.

[28]Gupta, R. N., Lee, K. P., Moss, J. N., Zoby, E. V., and Tiwari, S. N., "Viscous Shock-Layer Analysis of Long Slender Bodies," AIAA Paper 87-2487, Aug. 1987.

[29]Zoby, E. V., Lee, K. P., Gupta, R. N., Thompson, R. A., and Simmonds, A. L., "Viscous Shock-Layer Solutions with Nonequilibrium Chemistry for Hypersonic Flows Past Slender Bodies," AIAA Paper 88-2709, June 1988.

[30]Gnoffo, P. A., "Vectorized Finite-Volume, Adaptive Grid Algorithm Applied to Planetary Entry Problems," AIAA Paper 82-1018, June 1982.

[31]Vigneron, Y. C., Rakich, J. V., and Tannehill, J. C., "Calculation of Supersonic Viscous Flow Over Delta Wings with Sharp Subsonic Leading Edges," NASA TM-78500, June 1978.

[32]Gnoffo, P. A., "Hypersonic Flow Over Biconics Using a Variable-Effective-Gamma, Parabolized-Navier-Stokes Code," AIAA Paper 83-1666, July 1983.

[33]White, F. M., *Viscous Fluid Flow*, McGraw-Hill, New York, 1974.

[34]Sims, J. L., "Tables for Supersonic Flow Around Right Circular Cones at Zero Angle of Attack," NASA SP-3004, 1964.

[35]Ferri, A., "Some Heat-Transfer Problems in Hypersonic Flows," *Aeronautics and Astronautics*, Pergamon, New York, 1960, pp. 344-377.

[36]Rotta, N. R., "Effects of Nose Bluntness on the Boundary-Layer Characteristic of Conical Body of Hypersonic Speed," New York Univ., Rept. NY-AA-66-66, Nov. 1966.

[37]Kumar, A., Graves, R. A., and Weilmuenster, K. J., "Users Guide for Vectorized Code EQUIL for Calculating Equilibrium Chemistry on Control Data STAR 100 Computer," NASA TM-80193, April 1980.

[38]Singh, D. J., Kumar, A., and Tiwari, S. N., "Effect of Nose Bluntness on Flowfield Over Slender Bodies in Hypersonic Flows," AIAA Paper 89-0270, Jan. 1989.